Biosensors and Bioelectronics 312 (2026) 118986

Contents lists available at ScienceDirect

Biosensors and Bioelectronics

journal homepage: www.elsevier.com/locate/bios

Matrix tolerance, probe orientation, and antifouling interfaces in graphene biosensors

Kalyan Vaid [a,*], Indresh Verma [a], Vishnu Pullagantil [a], Radek Zboril [a,b], Aristides Bakandritsos [a,b,**]

[a] Regional Centre of Advanced Technologies and Materials, The Czech Advanced Technology and Research Institute (CATRIN), Palacký University, Šlechtitelů 27, Olomouc, Czech Republic

[b] Nanotechnology Centre, Centre for Energy and Environmental Technologies, VSB–Technical University of Ostrava, 17. listopadu 2172/15, Ostrava-Poruba, 708 00, Czech Republic

ARTICLE INFO

Keywords:
Graphene biosensors
Matrix tolerance
Probe orientation
Antifouling interfaces
Complex-matrix performance
Interface engineering
Biosensor stability

ABSTRACT

Graphene-based biosensors offer high analytical sensitivity, positioning graphene as a leading transducer material for next-generation environmental, food-safety, and biomedical diagnostic applications. As the field advances toward real-world implementation, maintaining performance in complex biological and environmental matrices remains a central challenge. Under these conditions, analytical reliability is governed not only by graphene's intrinsic properties, but also by the structural and functional organization of the bio-nano interface. This review examines recent interface-engineering strategies that address these challenges through three interconnected design parameters: matrix tolerance, probe orientation, and antifouling. We discuss how porous and nanostructured interfaces regulate mass transport and preserve signal integrity in minimally processed samples, how linker chemistry and surface architecture control the accessibility and presentation of biorecognition elements within the effective transduction zone, and how hydrated antifouling layers suppress nonspecific adsorption while stabilizing interfacial charge transfer. We further discuss multiparametric interface engineering as a unifying framework for improving selectivity, robustness, quantitative accuracy, and sensitivity. The review highlights critical design principles, benchmarking needs, and translational priorities for the development of graphene biosensors intended for clinical, environmental, and food-monitoring applications.

1. Introduction

Biosensors are increasingly important in modern health diagnostics, environmental monitoring, and food safety because of the growing demand for rapid, low-cost, point-of-care testing. Among emerging transducer materials, graphene occupies a unique position because of its exceptional electrical conductivity, atomic thickness, large specific surface area, stability, and chemical versatility. Several graphene or graphene derivatives based-biosensor platforms have reported femtomolar or sub-femtomolar limits of detection (LODs) under optimized buffer conditions; however, such metrics alone do not predict performance in real samples (Jakubec et al., 2025; Lee et al., 2019; Novoselov et al., 2012; Z. Wang et al., 2025).

Building on these advances, recent work has increasingly focused on translating graphene biosensors from controlled buffer environments to complex real-world matrices such as whole blood, serum, saliva, urine, food extracts, and natural or wastewater samples. These biological and environmental samples introduce substantial biochemical complexity because of their high protein content, ionic strength, viscosity, and electroactive interferents. Under such conditions, nonspecific adsorption, electrostatic screening, and diffusion limitations can cause signal attenuation, baseline drift, and reduced analytical reliability. Addressing these hurdles creates opportunities to engineer robust and tailored interfaces that preserve high sensitivity and specificity in minimally processed samples. Although graphene remains an ideal transducer, these challenges highlight that operational robustness depends not only on the graphene basal plane but also on the molecular architecture, function, and integrity of the bio-nano interface (Sackmann et al., 2014;

* Corresponding author.
** Corresponding author. Regional Centre of Advanced Technologies and Materials, The Czech Advanced Technology and Research Institute (CATRIN), Palacký University, Šlechtitelů 27, Olomouc, Czech Republic.
E-mail addresses: kalyan.vaid@upol.cz (K. Vaid), a.bakandritsos@upol.cz (A. Bakandritsos).

https://doi.org/10.1016/j.bios.2026.118986
Received 15 June 2026; Accepted 2 July 2026
Available online 6 July 2026

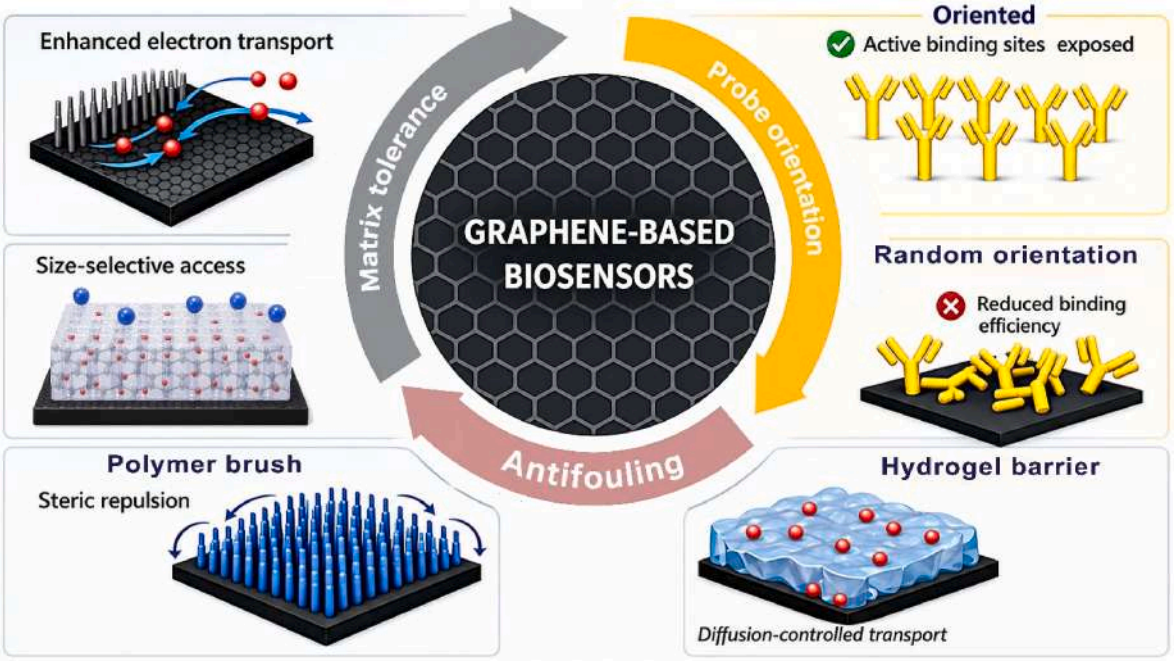

Fig. 1. Key design strategies at the bio-nano interface in graphene-based biosensors operating in complex matrices. The performance depends critically on the bio-nano interface, which can be optimized through three interdependent factors: matrix tolerance, probe orientation, and antifouling properties.

Turner, 2013; Zhu et al., 2025). Several studies highlight that refining interfacial architecture is essential for reliable analysis in clinical and real-sample settings (Parolo et al., 2020; Zhao et al., 2023). Successful operation in complex environments requires optimization of three interdependent design factors (Fig. 1): (i) tailored architectures, such as size-selective layers and selective binding pathways for matrix tolerance, (ii) oriented versus random antibody immobilization for binding efficiency and high sensitivity, and (iii) steric or diffusion-controlled surface-protection strategies that provide antifouling properties and minimize nonspecific adsorption, cross-reactivity, and signal interference. Together, these design principles support efficient electron transport, selective analyte access, and long-term interfacial stability, thereby improving the reliability of graphene-based biosensors in biological fluids and other complex matrices.

In this review, we examine recent advances in interface-design strategies structured around these three interdependent and complementary factors. The first, matrix tolerance, encompasses interfacial architectures that preserve analytical performance in complex or viscous fluids by tailoring the physicochemical environment at the graphene surface. The second, probe orientation, concerns the controlled immobilization of recognition elements so that their active sites are fully accessible to the solution phase with minimal denaturation. The third, antifouling, includes strategies such as zwitterionic (ZW) brushes and hydrogel barriers that suppress nonspecific adsorption, signal interference, and stabilize baseline signals (Parolo et al., 2020; Zhao et al., 2023). This review highlights the interrelated roles of these three factors in real-world biosensor performance and examines electrochemical and field-effect graphene platforms to show how matrix tolerance, probe orientation, and antifouling jointly influence stability, selectivity, and reproducibility in complex or minimally processed samples. By treating matrix tolerance, probe orientation, and antifouling as coupled interfacial design variables, this review provides a framework for understanding progress across graphene biosensing strategies and for identifying biointerface designs that sustain sensitivity, selectivity, and signal stability in clinically and environmentally relevant diagnostic settings.

2. The biointerfacial barrier

A central challenge in translating graphene-based biosensors from controlled laboratory buffers to complex biological matrices is biofouling at the sensor-matrix interface. In practical sensing environments, biofouling encompasses a spectrum of interrelated physical and chemical processes in which the nonspecific adsorption of proteins, lipids, and cellular debris leads to the formation of a biomolecular corona, or biofouling layer, on the graphene surface. This interfacial layer can mask or block the active probe-recognition sites, increase charge-transfer resistance (R_{ct}), and substantially reduce the signal-to-noise ratio.

Plasma and serum exposure can strongly attenuate sensor responses, but the magnitude depends on surface chemistry, assay format, incubation time, and readout mode (Liu et al., 2023). This section therefore distinguishes four mechanisms related to protein/corona formation, viscosity-controlled mass transport, electrostatic screening, and redox interference. In particular, biocorona formation initiates rapid albumin and fibrinogen adsorption within seconds, increasing R_{ct} from 100 Ω cm^2 to 10 kΩ cm^2 while blocking a substantial fraction of the conductive interface (Loo et al., 2013; Shahriari et al., 2026). In parallel, a three- to five-fold viscosity increase ($\eta \approx 4$ cP) can reduce analyte diffusivity, with D_{app} values approaching $\sim 10^{-6}$ cm^2 s^{-1} for representative biomolecules (as estimated from the Stokes-Einstein relation), which results in significant diffusion-induced deterioration in detection performance, and in concentration polarization at the electrode (Breault-Turcot and Masson, 2015; Echeverri et al., 2024; Khrapak and Khrapak, 2024).

Beyond these physical barriers, electrostatic screening and redox interference further compromise signal reliability. For example, physiological concentrations of uric acid (UA) and ascorbic acid (AA) generate overlapping voltammetric responses (±0.2 V vs. Ag/AgCl) near common oxidation windows, that can mask analyte-specific signals. At the same time, high concentrations of plasma electrolytes shorten the Debye length, and attenuate electrostatic coupling. Matrix-induced surface charges can also shift the graphene field-effect transistor (GFET) Dirac point by tens to hundreds of millivolts and amplify baseline noise to 15-30 mV h^{-1} (Demirkan et al., 2020; Meng et al., 2021;

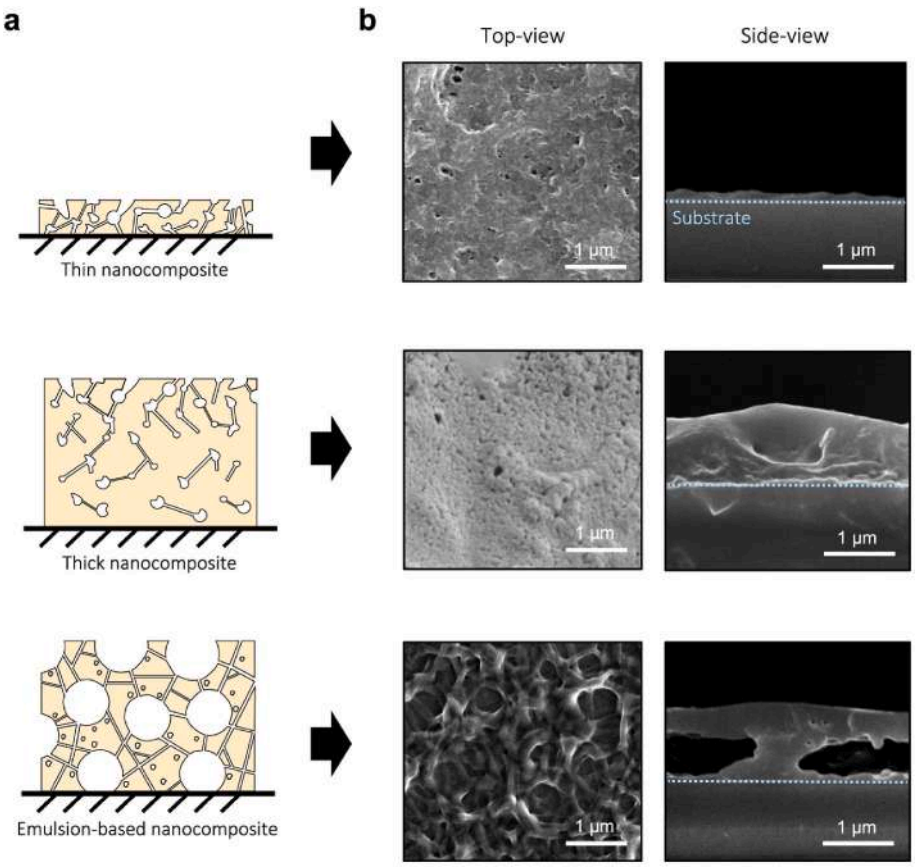

Fig. 2. (a) Schematic of three different cross-linked BSA nanocomposites: thin, thick, and porous emulsion-based nanocomposites. **(b)** Top- and side-view SEM images of nanocomposites. The three nanocomposites exhibited distinct coating thicknesses and porosities illustrating how architecture influences matrix tolerance (Reproduced from Lee et al., 2024).

Pellitero et al., 2021).

Because these processes act simultaneously, performance degradation in complex media cannot be addressed by targeting a single mechanism. Instead, it requires the concerted interplay between matrix composition, interfacial architecture, and signal transduction. While many studies have addressed individual aspects of biofouling or screening, a unified interface-design perspective remains necessary to understand and address these interdependent effects.

3. Interfacial design considerations in complex media

Active engineering of the bio-nano interface is essential to isolate the transducer from destructive, matrix-derived interferences. The following sections evaluate the primary methodologies used to regulate this interface by shielding the sensing surface from matrix effects while optimizing target recognition.

3.1. Matrix tolerance in complex biological environments

When graphene biosensors are translated from controlled laboratory conditions to clinical applications, undiluted matrices such as serum, saliva, and whole blood contain high concentrations of proteins, salts, and other biomolecules that can significantly impair signal stability and transduction efficiency. Achieving reliable outcomes therefore requires the strategic incorporation of structural and molecular elements that can increase matrix tolerance at the sensor interface and promote selective target recognition and efficient transduction. In this section, matrix tolerance is discussed as an interfacial property that emerges from structural, chemical, and electronic design choices over the graphene surface.

Passive exclusion is one practical strategy for mitigating matrix-induced interference. In this approach, porous interfacial architectures act as size-selective barriers that restrict the access of high-molecular-weight interferents, while preserving transport of smaller targets. Lee et al. compared three cross-linked bovine serum albumin (BSA) nanocomposite architectures (thin, thick, and emulsion-derived porous coatings, Fig. 2a) and showed how structural design directly influences matrix tolerance (Lee et al., 2024). The key distinction is whether the coating provides a continuous, analyte-permeable network. The corresponding top- and side-view scanning electron microscopy (SEM) images (Fig. 2b) reveal distinct thickness and porosity profiles, showing that the emulsion-templated coating forms an interconnected micron-scale porous structure, whereas the denser coatings provide fewer continuous transport pathways. By mitigating electrochemical resistance due to structural thickness through an internal graphene (Zupančič et al., 2021), or gold nanowire, percolation network, the porous architecture creates a selective and permeable microenvironment that shields the sensor from the biochemical complexity of raw clinical samples. After one month of storage/exposure in complex biofluids, the coating retained up to 88% of the interleukin-6 (IL-6) signal, demonstrating prolonged matrix tolerance and low signal drift in protein-rich media (Sabaté del Río et al., 2019). The porous network, tortuosity, and interfacial chemistry enabled the rejection of high-molecular-weight proteins (>10 kDa; $r_{stokes} \approx 3.5$ nm for BSA) while allowing the diffusion of smaller cytokines, thereby mitigating biocorona-associated signal attenuation.

As a transferable carbon-electrode example, Jarosińska et al. evaluated antifouling coatings (including silicate sol–gel layers, poly-L-lactic acid, and poly(L-lysine)-g-poly(ethylene glycol; PLL–PEG) on pencil graphite electrodes exposed to cell-culture conditions, providing a

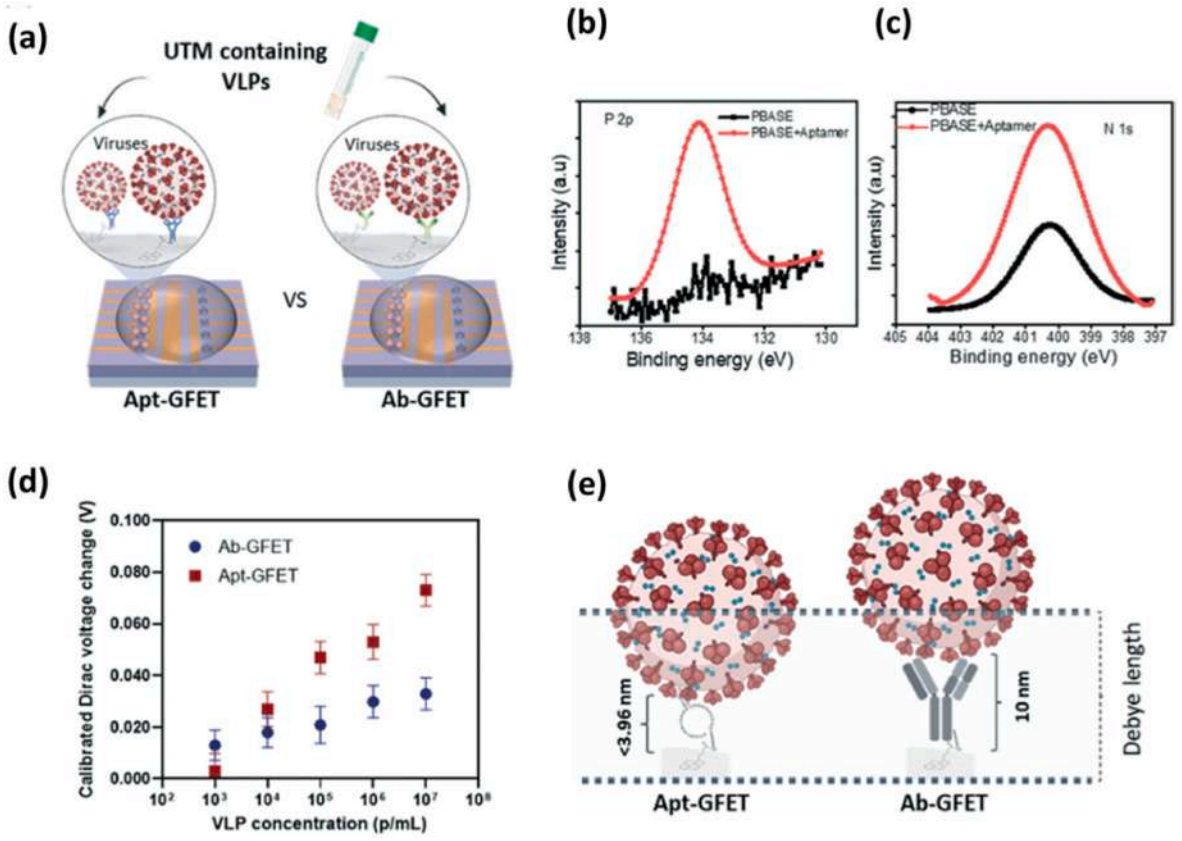

Fig. 3. Detection of SARS-CoV-2 in universal transport medium (UTM), used as a mock swab matrix, with an on-chip integrated graphene aptasensor (Apt-GFET, aptasensor): **(a)** the comparison schematic of the on-chip Apt-GFET biosensor (aptasensor) vs. the Ab-GFET one; **(b)** P 2p X-ray photoelectron spectroscopy (XPS) spectra; and **(c)** N 1s XPS spectra confirm the functionalization/attachment of aptamers on the graphene surface; **(d)** results of both sensors for SARS-CoV-2 virus detection in UTM; (e) the scheme showing the Debye screening effect for the Apt-GFET and Ab-GFET, as well as a comparison of the sizes of the antibody and aptamer. (Reproduced from Xu et al., 2022).

transferable model for matrix-tolerant carbon interfaces (Jarosińska et al., 2024). Using syringaldazine-modified pencil graphite electrodes as a model electrochemical interface, they showed that only a subset of coatings preserved the mediator response during prolonged incubation in cell culture medium. Among these, the TMOS-derived silicate sol–gel provided the longest-lasting protection: although the signal decreased by approximately half within the first 3 h, it remained detectable for up to 6 weeks. PLL–PEG also preserved well-defined syringaldazine peaks during cell-culture exposure, but its protective effect lasted for only about 2 weeks. These results indicate that silicate sol–gel protection is mainly associated with a porous, mechanically stable diffusion barrier, whereas PLL–PEG acts primarily through poly(ethylene glycol) (PEG)--mediated suppression of nonspecific adsorption. The study therefore supports the broader concept that matrix tolerance can be improved by interfacial coatings that preserve electrochemical readout while limiting fouling in complex biological environments.

Zinggeler et al. reported a printable, matrix-tolerant composite coating for screen-printed carbon electrodes based on a photoreactive copolymer containing conductive carbon nanotubes (CNTs). The rationale was to combine an antifouling matrix that suppresses protein adsorption with a crosslinked CNT percolation network that preserves charge transfer and further contributes to foulant exclusion through size- and diffusion-dependent transport. After printing, ambient drying, and rapid ultraviolet (UV) crosslinking, the optimized coating retained an electroactive surface area comparable to that of uncoated electrodes, but showed far greater fouling resistance. After 1 h of incubation in concentrated BSA, coated electrodes retained >90% of their initial electroactive surface area, whereas uncoated electrodes retained <20%. The same photocrosslinking chemistry was also used to immobilize capture antibodies, allowing biosensor fabrication in under 2 h. These functionalized electrodes were successfully used to quantify nanogram-range concentrations of inflammatory biomarker C-reactive protein (CRP) spiked in undiluted human blood serum (Zinggeler et al., 2022). This work demonstrates the value of interfaces that combine dual foulant-exclusion mechanisms – a polymer matrix and a CNT percolation network – with preserved charge transport.

A wafer-scale, on-chip integrated GFET aptasensor was developed for rapid, label-free detection of SARS-CoV-2 directly in universal transport medium (UTM), a clinically relevant electrolyte-rich matrix (Fig. 3a). This sensing platform used 1-pyrenebutanoic acid succinimidyl ester (PBASE) as a non-covalent functionalization layer to anchor the aptamer probes while preserving the electronic integrity of the graphene channel (Xu et al., 2022). The platform integrates a gold liquid-gate electrode into a wafer-scale GFET array, enabling stable operation in complex media without an external reference electrode. X-ray photoelectron spectroscopy (XPS) signals in the P 2p and N 1s regions confirmed successful aptamer immobilization on the graphene surface (Fig. 3b and c), and calibrated Dirac-voltage shifts demonstrated the superior sensitivity of the aptamer-functionalized GFET relative to antibody-based counterparts in UTM (Fig. 3d). This study highlights how probe size influences matrix tolerance under Debye-screening constraints. As illustrated schematically in Fig. 3e, the smaller dimensions of the aptamer (~3.96 nm) relative to antibodies (~10 nm) position the recognition event closer to the graphene surface, preserving effective signal transduction within the shortened Debye length of transport media. This architecture enabled the detection of virus-like particles at concentrations as low as ~10^3 particles mL^{-1} directly in UTM, demonstrating that controlled interfacial design and probe selection can

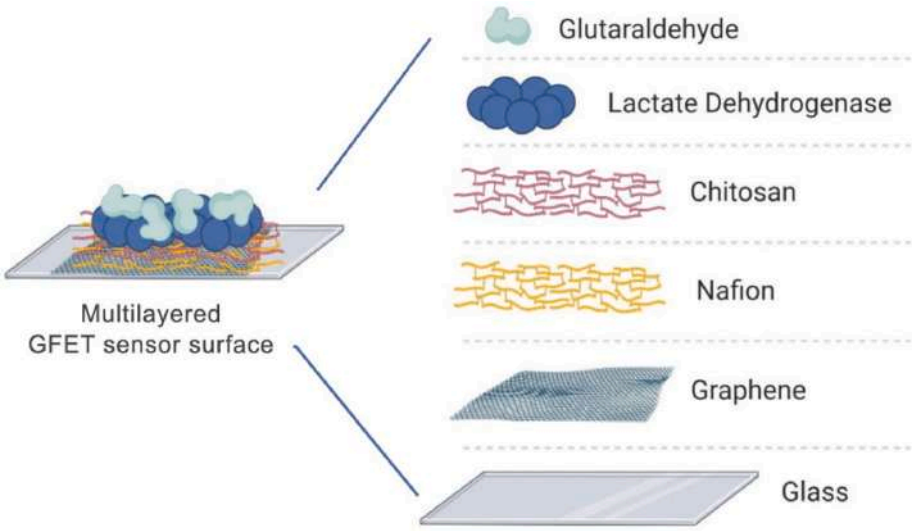

Fig. 4. Layered support for immobilizing lactate dehydrogenase on the graphene active layer of a GFET biosensor, enabling enhanced matrix tolerance. (Reproduced from Schuck et al., 2021).

maintain signal integrity in clinical matrices.

In a closely related GFET implementation, an engineered aptamer-functionalized device modified with a biomolecule-permeable PEG layer enabled cytokine detection directly in undiluted physiological media (Z. Wang et al., 2025). In this study, matrix tolerance arises from the combined effects of a passive exclusion layer, suppression of nonspecific adsorption, improved electrostatic coupling, and low-noise electrical readout. Aptamers were immobilized through pyrene-based succinimidyl ester chemistry (PASE/PBASE-type anchoring), in which the aromatic pyrene adsorbs onto graphene by π–π interactions and the activated ester reacts with amino-modified probes, thereby positioning the recognition element close to the graphene surface (Kumar et al., 2020; Z. Wang et al., 2025; Xu et al., 2022). The PEG layer simultaneously suppressed nonspecific adsorption and improved electrostatic coupling under high-ionic-strength conditions, thereby preserving charge sensitivity at the graphene interface.

By optimizing the PEG molecular weight (2000 Da) and controlling aptamer immobilization via PASE chemistry, the platform achieved LODs of 0.13 pM for tumor necrosis factor alpha (TNF-α) and 0.20 pM for interleukin-6 (IL-6) in undiluted artificial sweat and lavage fluid, with dissociation constants in the sub-nanomolar range. Notably, signal consistency between phosphate-buffered saline (PBS) and complex media (<10% KD deviation) demonstrated that matrix tolerance was achieved without compromising transduction efficiency. In parallel, the GFET architecture incorporated electronic noise-suppression strategies, achieving a signal-to-noise ratio of ~20 dB and a baseline drift of <2 mV h^{-1}. Stabilized Dirac-point tracking mitigated matrix-induced charge fluctuations, further enhancing operational robustness in ion-rich media.

Beyond these biological fluids, matrix tolerance has also been demonstrated in environmental waters using scalable graphene-film (GF) composite electrodes fabricated by roll-to-roll chemical vapor deposition (CVD) and transferred onto flexible polyethylene terephthalate (PET) substrates (Zhang et al., 2018). In this case, electrochemical oxidation introduced oxygen-containing groups for stable bioconjugation, whereas recovery tests in real water samples demonstrated matrix tolerance. The results validated the practicality and effectiveness of the macroscopic free-standing graphene architecture with a large electrochemically active surface area and mechanical robustness. These surface modifications improved analyte capture and reduced signal disruption from dissolved organic matter and metal ions in contaminated water. The resulting biosensors achieved a wide linear detection range (0.005-10 μg L^{-1}) and a low LOD of 2.3 ng L^{-1} for algal toxin detection in contaminated water. Validation in diverse real water samples yielded high recoveries (93-99%) with negligible interference from dissolved organic matter and metal ions (Zhang et al., 2018).

Among electrochemical implementations, chemical interface engineering provides another route to matrix tolerance. A silylated graphene oxide-based molecularly imprinted polymer (MIP), Si-GO-co-MMA/IA, was prepared from itaconic acid and methyl methacrylate and functionalized with vinyltrimethoxysilane to create uric-acid-specific nanocavities (Soman et al., 2023). Template removal generated selective binding sites that reduced interference from coexisting metabolites, while the graphene-containing matrix preserved a usable electrochemical baseline. The MIP-modified glassy carbon electrode achieved an LOD of 0.565 μM with good linearity ($R^2 \approx 0.93$) and allowed direct serum analysis without sample pretreatment. The selective nanocavity recognition underpinned matrix tolerance relative to the generic porous or antifouling overlayers discussed above.

While nanoporous layers provide a passive size, or diffusion-selective barrier against large biomolecules, excessive confinement can also impose diffusion constraints on the analytes. To address this trade-off, geometric engineering strategies (particularly vertically aligned graphene, VG architectures) have been developed to enhance mass transport while preserving interfacial accessibility. On a printed electrochemical platform based on VG modified with electrodeposited gold nanoparticles (VG@AuNPs), the high-density edge-plane structure (~2 μm height), together with the increased electroactive area, accelerated heterogeneous electron transfer and improved biomarker capture. This configuration enabled ultrasensitive detection of Alzheimer's disease blood biomarkers amyloid-beta (Aβ40 and Aβ42) and tau proteins (T-tau and P-tau181), with LODs down to 0.051 pg mL^{-1} in blood samples (Li et al., 2023), and the platform was validated using clinical samples. Here, the matrix interference was addressed mainly through serum dilution (which was possible due to the very low LOD of the sensor), BSA blocking, and selective antibody capture.

Advanced transistor engineering further reinforced matrix tolerance through a multiplexed solution-gated GFET in a common-gate configuration integrated with PDMS microchannels, thereby reducing device signal variability (mean Dirac voltage ~1 V, ±0.03 V). The architecture featuring coplanar Ti/Au electrodes bridged by CVD graphene and confined electrolyte channels was designed to control the sensing interface (Schuck et al., 2021). As shown in Fig. 4, the layered structure consisting of Nafion, chitosan, lactate dehydrogenase (LDH), and glutaraldehyde played unique roles at the interface. Nafion prevented the passage of anionic interferents such as urate and ascorbate, while

Table 1
Strategic approaches to enhance matrix tolerance in graphene-based biosensors.

Graphene Type	Interface Engineering Approach	Primary Mechanism	Key Performance Metric/Matrix	Ref.
Functionalized Graphene Oxide (GO) Flakes	Physical Exclusion	Cross-linked BSA-rGO porous matrix	Current retention after 60 min exposure to human serum, plasma, and whole blood; enabled sepsis biomarker detection in 50% whole blood	Zupančič et al. (2021)
Graphene Nanocomposites	Physical Exclusion	Sol-gel silicate/PLL-g-PEG grafting	50% signal retention for Redox Mediators after 6 weeks in cell culture medium	Jarosińska et al. (2024)
GO Nanoflakes	Physical Exclusion	Sacrificial BSA-templated printed matrix	Serum stability via albumin sequestration	Zinggeler et al. (2022)
Graphene FET	System Integration	Integrated readout electronics (Liquid-gate)	Rapid COVID-19 detection in UTM	Xu et al. (2022)
Graphene Film	System Integration	Interfacial cross-linking/robust bonding	Algal toxin detection in contaminated water; 93-99% recoveries in real samples	Zhang et al. (2018)
Vertical Graphene	Geometric Architecture	Edge plane exposure with AuNP decoration	Aβ42 & Phospho-tau in Human Serum LOD = 0.051 pg mL^{-1} in serum; 10–50-fold faster response kinetics.	Li et al. (2023)
GO-MIP Hybrid	Chemical Strategy	0.7 nm template nanocavities (silane layers)	Uric Acid in Human Blood Serum with >95% interferent rejection	Soman et al. (2023)
Graphene CGFET	Electronic Strategy	Common-gate potential stabilization	Stable L-lactic acid detection in human blood plasma	Schuck et al. (2021)
Graphene Aptasensor	Electronic Strategy	Multitransistor array signal averaging	Noise averaging and reduction for dopamine detection in brain fluids	Abrantes et al. (2022)
Graphene FET	Electronic Strategy	Effective Debye-length extension for serum-compatible FET readout	Specific IgE detection in undiluted, non-desalted human serum; LOD = 47 pM	Wang et al. (2018)
GFET Platforms	Electronic Strategy	Dirac point tracking & noise suppression	Plasma biomarkers in charge-screened plasma with SNR = 20 dB; drift <2 mV/h	Z. Wang et al. (2025)

chitosan and glutaraldehyde facilitated the immobilization of lactate dehydrogenase (LDH), and the confined microchannel design helped maintain the local electrolyte environment. In this platform, the analytical signal arises from enzyme-mediated changes in the local interfacial charge concentration and not from direct faradaic charge transfer through graphene, as in the case of electrochemical sensors. This configuration allowed linear lactate detection in plasma (0-7.5 mM; $R^2 \approx 0.98$) with minimal voltage shifts (<0.1 V) from UA, AA, and glucose, demonstrating enhanced matrix tolerance.

Alongside these interface-chemistry methods, multitransistor graphene array systems have been developed to enhance readout reliability through statistical averaging across multiple graphene transistors, reducing single-channel variability (Abrantes et al., 2022). The graphene multitransistor arrays (gMTAs), fabricated at wafer scale with nearly 80% yield, integrated 20 electrolyte-gated GFETs per 4.5 × 4.5 mm chip, enabling parallel replicate measurements from a single sample. Each channel was functionalized with a short dopamine-specific DNA aptamer via noncovalent π-π coupling chemistry, thereby preserving graphene's high carrier mobility while maintaining binding affinity within the Debye length. By averaging responses across multiple graphene channels, the platform suppressed device-to-device variability and filtered localized charge noise arising from matrix-induced ionic fluctuations. This configuration achieved an attomolar LOD (1 aM) with a dynamic range spanning 10 orders of magnitude (1 aM to 100 μM), together with a sensitivity of 22 mV per decade in artificial cerebrospinal fluid. Importantly, the array architecture preserved its sensitivity even in high-ionic-strength media and complex biological samples, including dopamine-depleted brain homogenates and 2 μL cerebrospinal fluid (CSF) samples from a Parkinson's disease model (Abrantes et al., 2022).

Wang et al. used an affinity graphene nanosensor for biomarker detection directly in undiluted human serum to illustrate an analogous method for enhancing matrix tolerance in graphene biosensors (Wang et al., 2018). A PEG nanolayer and an immunoglobulin E (IgE)-specific aptamer were successively functionalized in the graphene channel of a GFET using a PASE linker. This interfacial design served several functions; for example, the small aptamer helped keep the captured target within the electrostatically sensitive region of the device, while the PEG layer decreased nonspecific adsorption of background serum components, maintained access of serum-borne biomarkers to the recognition layer, and also extended the effective Debye screening length at the graphene surface. To further stabilize the electrical readout, biomarker capture was carried out in serum and the conductance measurement was subsequently performed in a conditioned low-ionic-strength PBS buffer, which improved control over ionic strength and pH during the FET measurement. By using IgE as a representative biomarker, the sensor achieved specific detection over a concentration range of 50 pM to 250 nM with a limit of detection of 47 pM in human serum. The sensing response was attributed to a combination of electrostatic gating by the positively charged IgE and conformational changes in the aptamer that brought electron-rich nucleotides closer to the graphene surface, thereby modulating channel conductivity.

Collectively, these studies show that matrix tolerance in graphene biosensors can be achieved by surface passivation along with engineering of the entire interfacial transport-and-transduction pathway. Porous nanocomposite and permselective coatings preserve electron transfer while restricting access of fouling macromolecules. The vertically structured graphene architectures increase the electroactive area and accelerate target transport while integrated liquid-gated or PEG-modified GFET platforms improve electrostatic coupling, suppress nonspecific adsorption, and stabilize signal output in high-ionic-strength media. The most effective designs regulate which species reach the interface, how efficiently binding occurs under diffusion and screening constraints, and how reliably the resulting perturbation is converted into a measurable electrical response. The strategies discussed in this section are summarized in Table 1. This reflects a shift from material-centered optimization to interface-integrated design, in which matrix compatibility emerges from the coordinated control of fouling, mass transport, electrostatics, and readout stability. It is also worth noting that matrix tolerance is not solely dependent on physical interfacial barriers; emerging electrochemical interrogation protocols such as frequency-tuned square-wave voltammetry and kinetic differential measurements can help deconvolute electron-transfer kinetics and correct for signal attenuation and baseline drift directly in whole blood (Dauphin-Ducharme et al., 2025).

Once these matrix-induced limitations are constrained and baseline preservation secured, the next major determinant of performance is the spatial organization of the biorecognition layer, specifically, whether

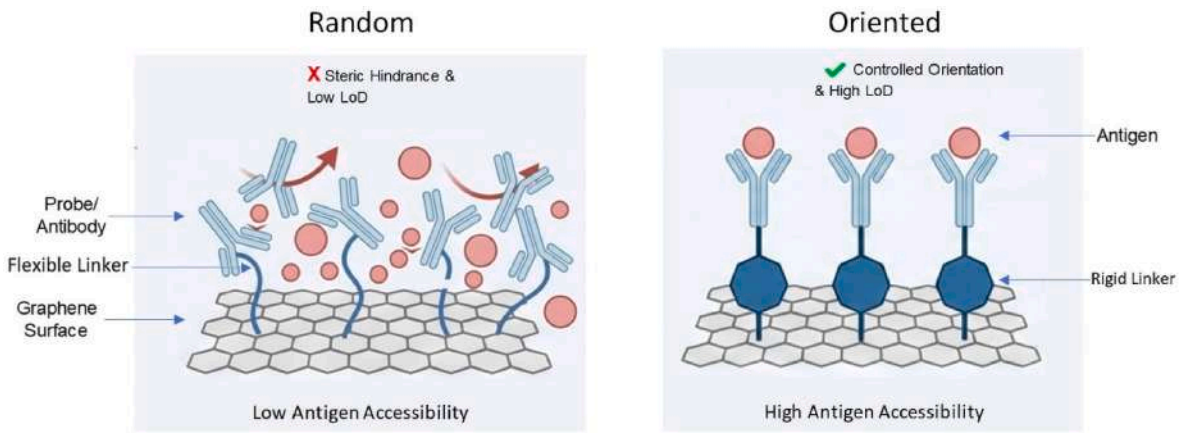

Fig. 5. Transitioning from conventional random probe orientation to a more accessible, oriented arrangement enabled by rigid linkers.

probes are positioned (oriented and spaced) so that target binding remains both sterically accessible and electrically coupled within the effective transduction zone.

3.2. Probe orientation and interfacial accessibility

Building on matrix tolerance, probe orientation represents another critical determinant of high-performance biosensor design. By controlling linker length, rigidity, and chemical functionality, researchers can mitigate site masking and diffusion limitations through more controlled immobilization. Effective analyte recognition depends on the spatial exposure, surface density, and conformational integrity of immobilized probes, which directly influence biomolecular accessibility, binding kinetics, and the LOD. Although graphene's honeycomb lattice offers a large surface area for immobilization, its chemical inertness does not prevent nonspecific physisorption, for example through hydrophobic interactions (for pristine graphene), or electrostatic and hydrogen bonding in the case of the functionalized graphene derivatives. Such random adsorption may cause denaturation of the biomolecular probes, steric hindrance, or recognition events that occur beyond the effective Debye screening length (critical for the GFET sensors), reducing transduction efficiency in biological media. Recent studies therefore emphasize rational linker engineering, site-specific conjugation, and nanostructured scaffolding to optimize probe orientation while maintaining effective electronic coupling with the graphene surface (Ramadan et al., 2021).

To preserve graphene's high carrier mobility while maintaining the integrity of the sp^2 lattice, noncovalent functionalization via π-π stacking remains widely adopted. Among these approaches, PBASE is commonly used to anchor biomolecules on graphene. However, density functional theory (DFT) analyses by Oishi et al. indicate that PBASE can adopt two locally stable conformations on graphene. A straight configuration, in which both the pyrene and butanoic acid succinimidyl ester (BSE) segments lie flat, and a bent configuration, in which the BSE moiety extends away from the surface. Under vacuum conditions, the flat configuration exhibits higher adsorption stability, reflecting the dominant contribution of the pyrene unit. The flexible alkyl chain of PBASE therefore introduces conformational variability that may influence how attached antibodies are spatially oriented. Importantly, the study further shows that environmental factors, such as hydration and proximal amino acids, can stabilize the upright conformation, highlighting that linker orientation is context-dependent. These findings suggest that commonly used flexible pyrene linkers may not consistently ensure optimal probe presentation, motivating the exploration of more structurally defined anchoring strategies to enhance interfacial accessibility (Oishi et al., 2022).

To overcome the limitations of flexible pyrene linkers, recent studies have employed rigid architectures, most notably those based on porphyrin macrocycles such as tetrakis(4-carboxyphenyl)porphyrin (TCPP). Unlike PBASE, whose flexible alkyl chain permits multiple adsorption geometries, TCPP forms an extended π-π network with graphene through its planar porphyrin core, while its peripheral phenyl rings tilt away from the surface. This geometry promotes directional coupling and favors a predominantly end-on antibody configuration (Yin et al., 2025). As shown schematically in the oriented and random panels of Fig. 5, rigid linkers reduce probe crowding and improve antigen accessibility relative to flexible PBASE-modified surfaces. This structural modification has been reported to improve the LOD of GFETs by at least two orders of magnitude (Ramadan et al., 2021; Yin et al., 2025).

The precision of molecular architecture, particularly the length and chemistry of linkers at the nanoscale, becomes especially important in high-ionic-strength physiological fluids, where the Debye screening effect imposes a major limitation. In electrolyte-rich media, the Debye length relevant to GFET transduction often falls within a few nanometres, such that electrical responses are dominated by charge perturbations occurring very near the graphene surface (Kumar et al., 2020). The molecular architecture must therefore ensure that recognition events occur within the electrostatic gating region of the graphene channel. Because electrostatic charge-carrier modulation is strictly confined within this nanoscale region, precise control over linker functionalization and probe orientation is a major determinant of field-effect sensitivity, alongside graphene quality, device noise, and readout architecture (Béraud et al., 2021).

This constraint has motivated the use of compact, vertically oriented probes such as RNA or DNA aptamers, typically extending around 2-3 nm from the surface when tethered through short pyrene linkers. For the GFET aptasensor reported by Wang et al., the 8-17 DNAzyme was functionalized with a pyrene linker at the 5' end, allowing the DNAzyme to anchor firmly via π-π stacking, where pyrene rings align and overlap with the carbon lattice of the graphene. This standing orientation prevents the DNA from lying flat and denaturing, and helps preserve the active DNAzyme conformation and its ability to bind lead (Pb^{2+}) ions effectively. This resulted in a ~4.5 nm increase in interfacial height, confirmed by atomic force microscopy (AFM). The obtained height was consistent with an upright configuration (instead of a flat) indicating a surface-accessible 8-17 DNAzyme probe layer. The device achieved an LOD of 37.5 ng L^{-1} for Pb^{2+} in complex matrices and demonstrated reliable operation in real blood samples, confirming that electrostatic transduction remains effective when probe geometry is tightly regulated (Wang et al., 2016).

Further control over vertical alignment and noncovalent immobilization is crucial for clinical translation. In salivary cortisol sensing, graphene foam electrodes were first modified with PBASE, whose

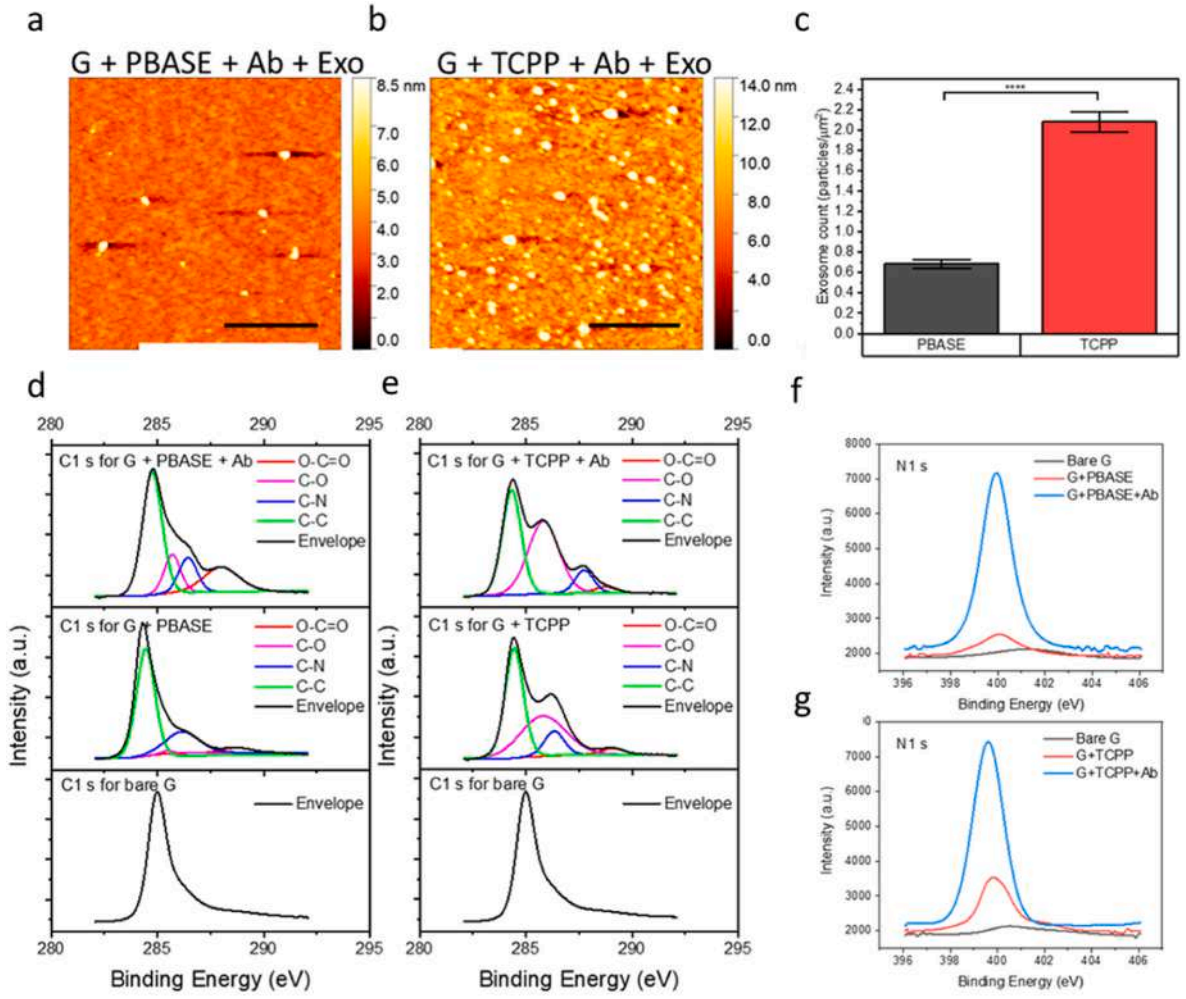

Fig. 6. Characterization of graphene functionalization and exosome capture efficiency. **(a, b)** AFM height images and **(c)** corresponding exosome density quantification on GFET surfaces modified with PBASE and TCPP linkers. TCPP surfaces show a ~3-fold increase in capture density (2.1 vs. 0.7 particles μm-2) compared to PBASE. **(d–g)** XPS C 1s and N 1s spectra confirming successful antibody immobilization via amide bond formation (399.8 eV) for both linkers. Despite comparable antibody loading, TCPP-based sensors achieve a two-order-of-magnitude improvement in LOD. This enhanced performance is attributed to the rigid TCPP porphyrin structure, which enforces an accessible end-on vertical antibody orientation, whereas the flexible PBASE alkyl chain results in disordered, sterically hindered configurations. Scale bars: 1 μm. (Reproduced from Yin et al., 2025).

pyrene moiety adsorbs on graphene while the succinimidyl ester couples to amino groups on the antibody (Sharma et al., 2024). Combined with the three-dimensional foam topography, this chemistry positioned the antibody layer away from the conductive scaffold and favored a vertically accessible recognition zone. This configuration yielded an ultrasensitive LOD of 0.24 fg mL^{-1} and showed strong agreement with enzyme-linked immunosorbent assay (ELISA) measurements ($r = 0.9961$), validating the architectural strategy in real human saliva.

Yin et al. studied the detection of exosomes following a 15-min incubation of 10^7 particles μL^{-1} of exosomes on PBASE-modified graphene, as well as on TCPP-modified graphene, both of which were biofunctionalized with antibodies. The AFM height profiles supported that after incubation, TCPP-modified surfaces exhibit a threefold higher exosome capture density (2.1 vs. 0.7 particles μm^{-2}) than PBASE-modified interfaces. These results demonstrate that the interfacial organization is crucial in determining the efficiency of analyte capture (Fig. 6a and b). This enhancement (quantified in Fig. 6c) is attributed to the rigid porphyrin macrocycle of TCPP, which positions antibodies toward a vertical end-on orientation that maximizes binding site accessibility. XPS data (Fig. 6d–g) supported comparable antibody loading on the two surfaces, indicating that the improved capture is more consistent with differences in orientation than with probe density alone. Although both linkers exhibit comparable antibody loading, as evidenced by the N 1s peak at 399.8 eV, TCPP-based sensors achieve a two-order-of-magnitude improvement in LOD. Thus, the performance gains are best explained by spatial orientation and not by differences in probe density (Yin et al., 2025). Together with theoretical modelling, the experimental results support the superiority of rigid linkers over flexible pyrene linkers for promoting accessible antibody orientation. The studies by Ramadan et al. and Yin et al. demonstrated that vertical probe alignment produced a threefold increase in capture density compared with flexible PBASE-modified surfaces for exosome capture (Ramadan et al., 2021; Yin et al., 2025).

Validation of these orientation strategies requires further advances in analytical characterization. Techniques such as time-of-flight secondary ion mass spectrometry (ToF-SIMS) combined with PCA can support antibody-orientation assignments when validated domain-specific fragment markers and controls are used (Yin et al., 2025). This evidence is increasingly complemented by DFT simulations and atomic force microscopy (AFM), where height increments (e.g., ~2.5-3 nm for RNA aptamers) can support oriented attachment when combined with chemical and functional controls (Kumar et al., 2020; Oishi et al., 2022; Yin et al., 2025). Furthermore, XPS helps verify surface chemistry and comparable probe loading, while orientation must be

Table 2
Interfacial engineering strategies for optimized probe orientation and signal transduction in graphene-based biosensors.

Graphene Type	Primary Mechanism	Key Performance Metric/Matrix	Ref.
Monolayer Graphene	1-pyrenebutanoic acid succinimidyl ester (PBASE)	Lowest adsorption energy (−1.63 eV) for flat configuration	Oishi et al. (2022)
CVD Graphene	Rigid Porphyrin (TCPP) vertical linkers	2 orders of magnitude LOD improvement; Vertical antibody alignment	Yin et al. (2025)
CVD Graphene	Carbon dot (CD) decoration	1000-fold SNR improvement vs non-decorated; Exosomes in serum	Ramadan et al. (2021)
CVD Monolayer	PBASE non-covalent RNA aptamers	$K_D \approx 70$ pM; multi-disease biomarkers in clinical saliva	Kumar et al. (2020)
Graphene/rGO	Au-hybrid nanoelectrode arrays	LOD: 10 fM (DNA); Electrical property optimization	Lee et al. (2019)
Exfoliated Graphene	8-17 DNAzyme functionalization	LOD: 37.5 ng/L; Portable lead detection via FET	Wang et al. (2016)
Graphene Foam (GF)	PBASE-NHS vertical antibody alignment	LOD: 0.24 fg/mL; strong correlation ($r = 0.99$) with ELISA	Sharma et al. (2024)
GO/rGO/ Nanocarbons	PEGylation & Lubricin (LUB) coatings	LOD: 23 pg/mL (IL-6) in undiluted plasma	Russo et al. (2021)
Laser-scribed Graphene (LSG)	Sulfobetaine-zwitterionic (ZW) moieties	>90% signal preservation after 24 h biofouling exposure	Zambrano et al. (2024)

inferred from complementary structural and functional measurements. Electrochemical methods such as electrochemical impedance spectroscopy (EIS) and cyclic voltammetry (CV) remain important indirect tools for evaluating probe presentation, conformational accessibility, and overall sensor performance (Zambrano et al., 2024).

All these advances indicate that achieving a high-performance interface requires a careful balance between molecular architecture and multimodal experimental validation of results. A comprehensive benchmarking of the gains produced by molecular scaffolding and spatial-orientation strategies is presented in Table 2, highlighting the close relationship between interfacial organization and ultralow LOD. However, oriented probes remain vulnerable to gradual fouling and adsorption-driven masking, motivating the development of antifouling interfaces that preserve accessibility over time.

3.3. *Antifouling strategies for interfacial stability*

On graphene, nonspecific adsorption of proteins, lipids, and polysaccharides blocks recognition sites, perturbs local charge distributions, and changes ion/electron transport near the transducer surface (Lee et al., 2019; Y.-T. Wang et al., 2025). The practical consequence is a drift from the nominal sensitivity measured in a synthetic buffer toward weaker, less stable signals in real samples. To mitigate such issues, the antifouling design is essential to prevent sensitivity loss in protein-rich or cell-rich samples. The antifouling strategies discussed below are therefore critical for preserving target accessibility and maintaining a stable signal response (Russo et al., 2021).

Initial efforts to mitigate fouling at the bio-nano interface focused on establishing hydration barriers using neutral hydrophilic polymers such as PEG, polyvinyl alcohol (PVA), and polysaccharides without fundamentally compromising signal transduction (Ilyas et al., 2019; Russo et al., 2021; Saxena et al., 2024). These coatings increase surface wettability, effectively masking the hydrophobic nature of graphene and reducing water contact angles from >110° to below 40° (Ilyas et al., 2019). Multiple studies suggest that PEGylation significantly improves resistance to nonspecific binding. In membrane and coating studies, PEGylation can yield flux-recovery ratios above 90% in protein-rich environments, although biosensor signal retention must be benchmarked separately (Saxena et al., 2024). Their main limitation is that the same hydration barriers can also slow down analyte transport and, if these barriers become too thick or chemically unstable, they can attenuate electrochemical or field-effect responses in complex biofluids. For this reason, current antifouling design has shifted toward strongly hydrated interfaces that combine fouling resistance with better control over interfacial transport of target analytes (Russo et al., 2021). Among these interfaces, ZW polymer brushes such as poly(carboxybetaine) and poly(sulfobetaine) represent some of the most effective solutions for molecular-scale antifouling. Unlike PEG, which relies primarily on hydrogen bonding, zwitterions incorporate equimolar cationic and anionic groups that form tightly bound hydration layers through strong ion-dipole interactions (Liu et al., 2020). This water barrier creates a significant thermodynamic penalty for its displacement by proteins, rendering nonspecific adsorption unfavorable even under high ionic strength conditions. Molecular-level investigations have further shown that these brushes exhibit higher water coordination numbers and longer residence times than conventional polymers.

In practical applications, the utilization of sulfobetaine-zwitterion-functionalized laser-scribed graphene (LSG) can preserve more than 90% of the signal after 24 h of exposure to high-protein media (Fig. 7). The study used fluorescence microscopy, SEM, and differential pulse voltammetry (DPV) to support this conclusion. The fluorescence intensity on the bare electrode (LSGE) was higher than on the modified electrode (LSGE/ZW), indicating greater albumin adsorption on the unmodified surface (Fig. 7a). Fig. 7b further shows approximately 80% lower fluorescence for the modified electrode. The SEM images reveal that adsorbed albumin spreads across and blocks the porous structure of bare LSGE to a much greater extent than that of LSGE/ZW, explaining the pronounced loss of current density and electroactive area (Fig. 7c).

The adhesion of BSA, *E. coli*, and HeLa cells to the bare electrode, together with the anti-adhesion properties of the modified electrode, is shown in Fig. 7d, which demonstrates the superior sensitivity preservation of the ZW interface. Fig. 7e differentiates the electrochemical behavior of the PEG-modified electrode from that of the zwitterion-modified electrode, confirming that the ZW approach is more robust. The ZW film remains permeable to small redox probes and, unlike bare or PEG-modified electrodes after albumin exposure, it resists formation of a dense protein-blocking overlayer. This implies that the coating excludes macromolecular foulants more effectively than it excludes the electroactive species used for readout. Furthermore, Jashrapuria et al. introduced surface-initiated atom transfer radical polymerization (SI-ATRP) as a route to graft polymeric brushes with tunable density and thickness (Jashrapuria and Singh, 2023). This method helps to maintain a more homogeneous nano-bio interface, minimizing local charge variations that would otherwise disrupt field-effect transduction or electron-transfer kinetics.

To extend this strategy to the mesoscale, 3D architectures such as hydrogels and nanochannel membranes have emerged as effective barriers, particularly during prolonged exposure to complex media. As summarized schematically in Fig. 8, relative to a bare graphene surface (Fig. 8a), these architectures can be grouped into three broad formats: (i) hydrated polymer networks that provide steric exclusion (Fig. 8b), (ii) zwitterionic polymeric brushes (Fig. 8c) that can be enhanced with conductive components that retain charge transport, and (iii) nanochannel systems that filter transport by size and charge (Fig. 8d). Hydrogel-graphene nanocomposites, such as PVA-sodium alginate-graphene oxide (PVA-alginate-GO) systems, use highly hydrated polymer networks to provide steric hindrance against large foulants (Amiri et al., 2020). These hydrogels have been shown to limit the BSA-induced flux decline, demonstrating that graphene can be effectively shielded without sacrificing inherent transduction sensitivity. Hybrid conductive barriers partially address this trade-off. For example, $Ti_3C_2T_x$

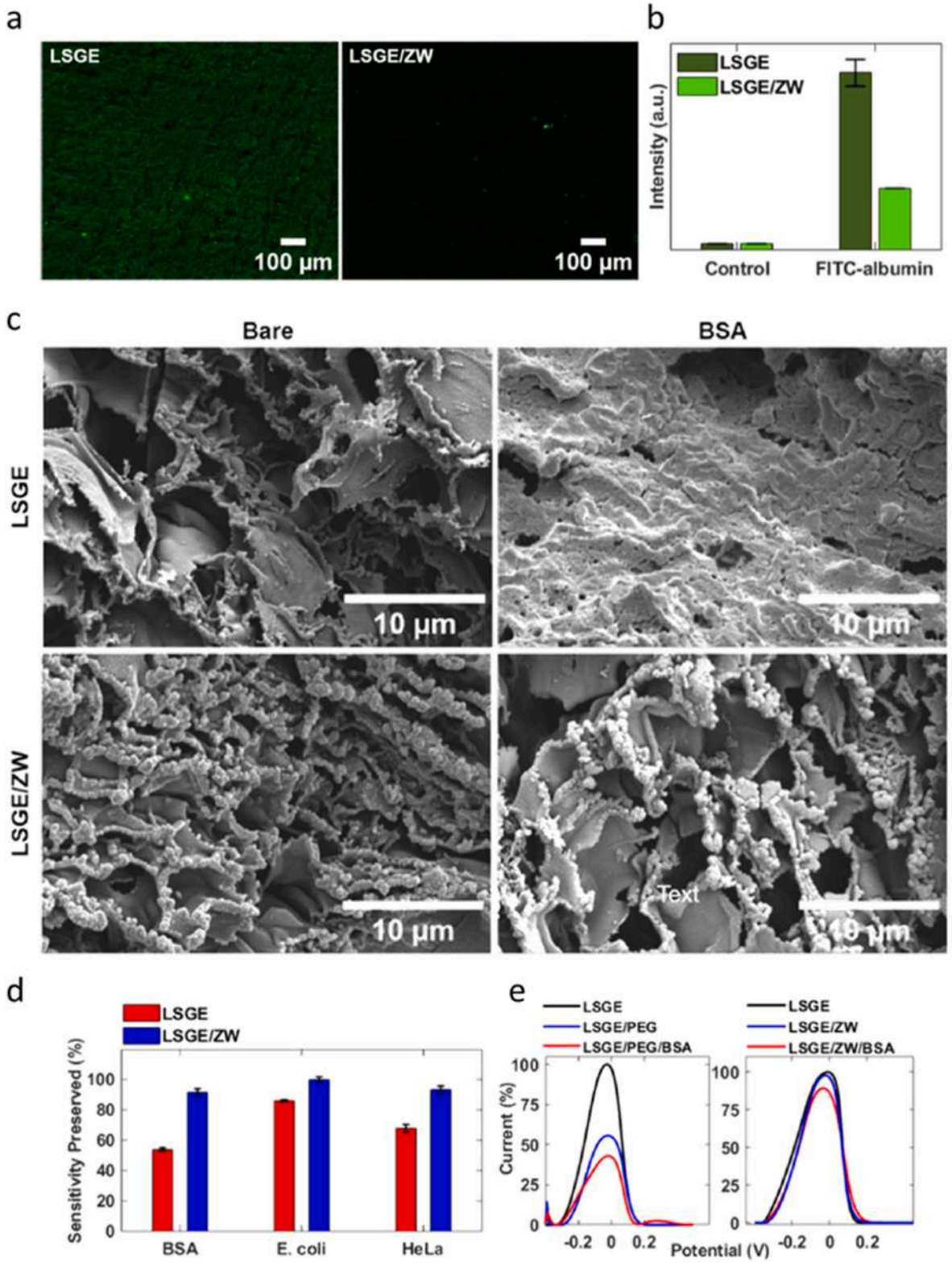

Fig. 7. **(a)** Fluorescence microscopy images of bare LSGE and LSGE/ZW after 24 h of immersion in 10 mg mL^{-1} fluorescein-albumin solution. **(b)** Fluorescence intensity comparison between LSGE and LSGE/ZW before and after 24 h of immersion in 10 mg mL^{-1} fluorescein-albumin (FITC-albumin). **(c)** SEM images of bare LSGE and LSGE/ZW before and after immersion in 10 mg mL^{-1} albumin solution (BSA). **(d)** Sensitivity-preserved percentages of bare LSGE and LSGE/ZW after 24 h of incubation with albumin, *E. coli* bacteria, and HeLa cell incubation. (n = 4 independent electrodes). **(e)** Differential pulse voltammograms of LSGE/PEG and LSGE/ZW in a supporting electrolyte containing 5.0 mM $K_3[Fe(CN)_6]/K_4[Fe(CN)_6]$ in 0.1 M KCl. Original peak current response (black) and functionalized electrodes (blue) after 24 h of immersion in 10 mg mL^{-1} albumin solution (red) (n = 4 independent electrodes). Reproduced from: (Zambrano et al., 2024). (For interpretation of the references to colour in this figure legend, the reader is referred to the Web version of this article.)

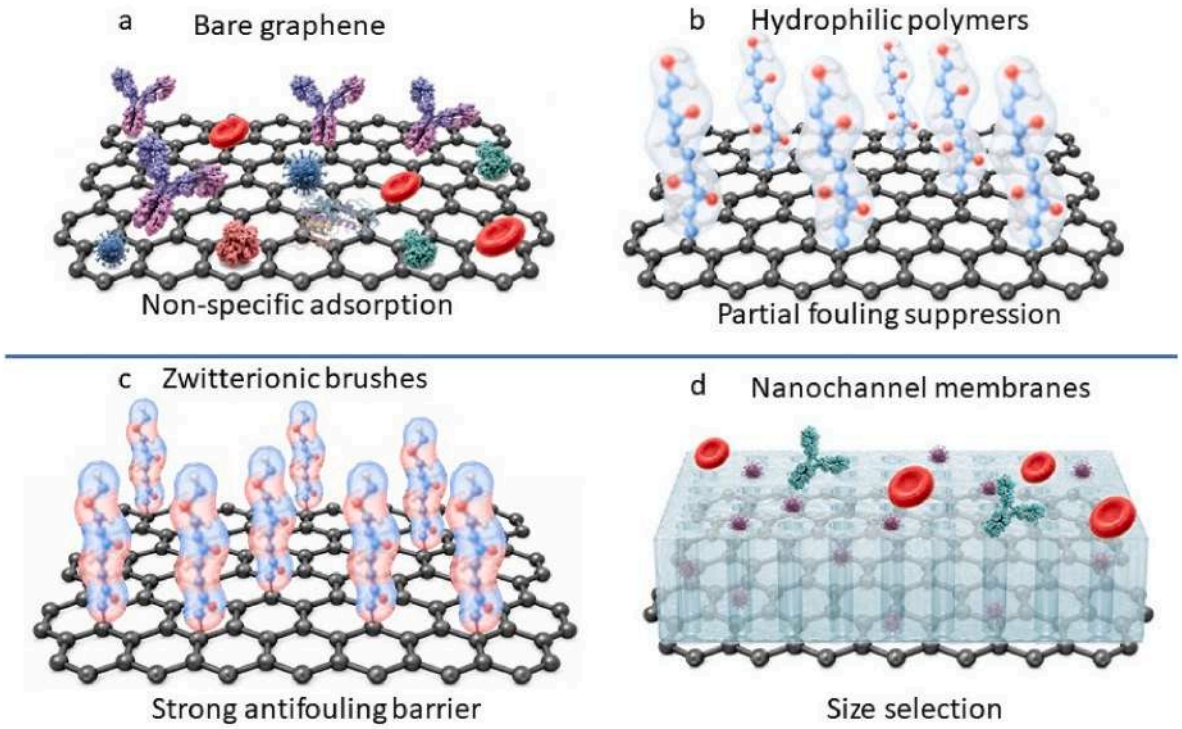

Fig. 8. Antifouling surface architectures for graphene-based biosensing in complex media. **(a)** Nonspecific adsorption of proteins, cells, and other matrix components on an unprotected graphene surface. **(b)** Polymer hydrophilic coatings that induce a steric hydration barrier. **(c)** Strongly hydrated zwitterionic brush-type coatings enable interfaces that resist protein adsorption. **(d)** Vertical hydrogel or nanochannel barriers that regulate analyte transport by size and diffusion path length.

Table 3
Benchmarking antifouling strategies and interfacial resilience.

Graphene Type	Strategy Category	Primary Mechanism	Matrix/Testing Environment	Key Performance Metric	Ref.
Graphene Oxide (GO)	Hydrophilic Coating	PEG-functionalized GO-Ag additive	BSA protein solution (Model Fouling)	91.3% flux recovery ratio; water flux: 906 L m^{-2} h^{-1} in BSA	Ilyas et al. (2019)
Pristine Graphene	Probe Orientation	TCPP Porphyrin rigid linker	Pancreatic cancer exosomes in serum	2 orders of magnitude LOD improvement; Structural order reduces fouling	Yin et al. (2025)
Various Graphene	Hybrid Composite	Hydrogel/Zwitterionic coatings	Whole blood and undiluted plasma	20–23 pg/mL LOD (TNF-α/IL-6); optimized for electrochemical sensing	Russo et al. (2021)
Various Graphene	Polymer/Peptide	PEG, zwitterions, and peptides	Clinical matrices (Serum/Saliva)	LOD: 3 fM (mRNA-21); High specificity in clinical matrices	Saxena et al. (2024)
N/A (Simulation)	Molecular Control	pCBMA/pSBMA Molecular Simulations	Blood serum and plasma (Simulated)	Protein adsorption <7.5 ng/cm^2; mechanistic water-barrier validation	Liu et al. (2020)
Graphene Oxide (GO)	Zwitterionic Brush	pMEDSAH grafting via SI-ATRP	Bacterial suspension (*E. coli*)	~90% decrease in live biomass; Resistance to *E. coli* fouling	Jashrapuria and Singh (2023)
TACeMGO Sheets	Zwitterionic Brush	PSBVI dual-crosslinked hydrogel	Artificial Seawater (Microalgae)	Settlement reduction of spores; Modulus increase to 7.30 × 10^{-2} GPa	Wang et al. (2023)
rGO/ZnO	Polyampholyte	Hydrogel surface grafting on PES	Synthetic Wastewater (EfOM)	Minimal TMP increase in wastewater; Inhibition of *P. aeruginosa*	W. Zhang et al. (2022)
Graphene Oxide (GO)	3D Hydrogel	PVA-GO-NaAlg blended matrix	Dye-rich wastewater & BSA	>83% dye rejection; Steric exclusion of BSA proteins	Amiri et al. (2020)
Graphene Oxide (GO)	3D Hydrogel	PVA-SA-GO nanocomposite layer	Arsenic-contaminated water	88.4% As(III) removal; permeability of 15.8 L m^{-2} h^{-1} bar^{-1}	Amiri et al. (2023)
Holey Graphene (HG)	Mesoscale Barrier	$Ti_3C_2T_x$ MXene hybrid interface	Undiluted Human Serum	85.9% signal retention after protein immersion; Dopamine in serum	L. Zhang et al. (2022)
Graphene Oxide (GO)	Biomimetic Hybrid	MGO Core-sheath + Cerium-polyphenol	Corrosive NaCl (3.5 wt%)	96.4% self-healing efficiency; impedance stability in corrosion	Li et al. (2025)

MXene-holey graphene interfaces combine high hydrophilicity with conductive transport pathways, preventing graphene restacking and retaining ~86% of the electrochemical response after BSA exposure in serum-relevant testing (L. Zhang et al., 2022). Silica nanochannel membranes represent a complementary rigid architecture. Vertically aligned mesoporous silica films with nanometer-scale channels can act as permselective antifouling layers, excluding larger foulants while allowing smaller analytes to reach the underlying transducer (Gong et al., 2021; Lv et al., 2022) .

These rigid frameworks offer better resistance to swelling and oxidative degradation than polymer-based systems, although precise control over channel length is still required to avoid hindering electron transfer. High-performance ZW polymers such as poly(carboxybetaine methacrylate) (pCBMA) and poly(sulfobetaine methacrylate) (pSBMA), show among the strongest predicted antifouling performance in molecular simulations, whereas MXene–graphene hybrids and ZW brushes

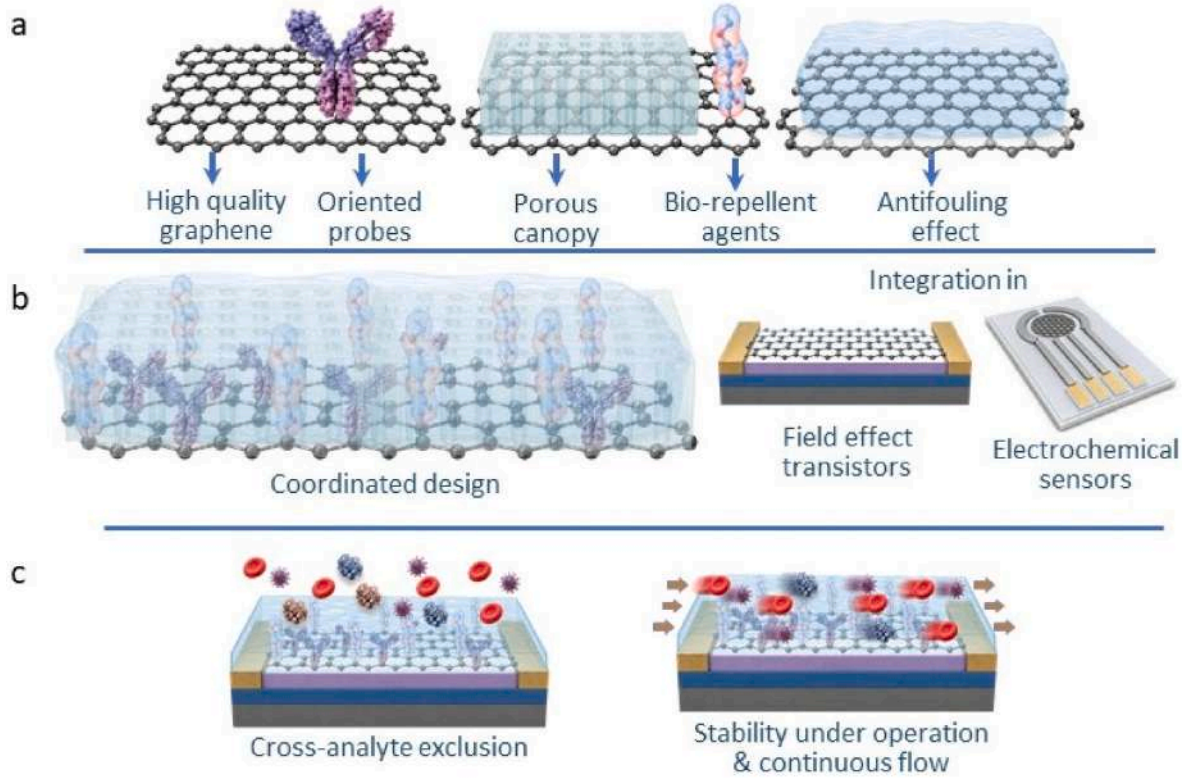

Fig. 9. Coordinated interfacial design in graphene-based biosensors. **(a)** Schematic of a graphene-based biosensor interface illustrating the individual components: high-quality graphene, oriented probes, a porous canopy, and bio-repellent agents that together form an antifouling interface. **(b)** The coordinated design integrating these elements, which can be applied to both field-effect transistor (FET) and electrochemical sensor platforms to support enhanced signal stability. **(c)** Demonstration of the functionality of the coordinated interface under complex biological conditions, highlighting cross-analyte exclusion and stability under continuous flow.

provide the most robust experimentally demonstrated solutions (Liu et al., 2020). To highlight transferable antifouling design principles, Table 3 includes both biosensor-focused strategies and selected cross-domain examples (e.g., membrane-based systems), which are discussed here for their mechanistic relevance.

4. Coordinated interfacial engineering

Recent advances in graphene-based biosensors show that performance in complex media depends on the combined optimization of transport, probe accessibility, and fouling resistance. This shift from single-parameter refinement to coordinated interface engineering is essential for maintaining signal integrity.

As shown in Fig. 9a, the coordinated design for graphene-based biosensors can be conceptualized as multilayered systems in which porous canopy, oriented probes, and bio-repellent agents that form eventually antifouling layers function as a unified interfacial ensemble above a high-quality graphene platform. Porous or nanostructured matrices regulate the access of analytes and interferents, oriented bioreceptors maximize binding-site exposure within the effective transduction zone, and antifouling coatings preserve those gains during matrix exposure (Li et al., 2023). In this unified framework, robust matrix tolerance is not an isolated parameter, but rather a key analytical outcome achieved when a protective antifouling layer successfully repels non-specific interferents without compromising the precise probe orientation required for optimal target capture.

The evolution from isolated to coordinated interfacial strategies is highlighted in Fig. 9b, demonstrating the integration of these designs into field-effect transistors (FETs) and electrochemical sensors. While porous scaffolds (Lee et al., 2024), vertical probe orientation and accessibility (Yin et al., 2025), and ZW coatings that preserve electrochemical response after protein exposure (Zambrano et al., 2024) contribute independently to performance gains, their integration yields substantially improved signal stability. By simultaneously addressing matrix tolerance, probe accessibility, and hydration-layer stabilization, these unified designs maintain performance under protein-rich conditions. Beyond surface anchoring, the structural evolution of the recognition element itself is crucial; for instance, high-throughput array platforms are now being utilized to isolate structure-switching aptamers that maintain high specificity and favorable spatial orientation even in the presence of structurally analogous competitive interferents in complex samples (Fujita et al., 2025).

The practical implication is that sensor architectures must remain effective as matrix complexity increases from buffer to minimally processed biofluids and, ultimately, to continuous or repeated exposure conditions. Extending this perspective, Fig. 9c depicts the functionality of these coordinated designs under increasingly demanding operating conditions, highlighting cross-analyte exclusion and stability under continuous flow. For example, while a porous BSA-glutaraldehyde (GA) matrix can protect the sensing region for prolonged measurements in static plasma by effectively rejecting interferents, longer-term dynamic operation requires an additional low-fouling strategy to prevent the gradual accumulation of small molecules and proteins within the pores (Lee et al., 2024). This transition from static protection to longer-duration dynamic operation can be achieved by combining nanoporous encapsulation with chemical antifouling. The addition of agents such as β-cyclodextrin can improve performance under continuous flow by preventing the accumulation of small-molecule foulants, thereby extending the sensor's lifetime (Majeed et al., 2025).

Conceptual adaptation from studies on non-carbon electrochemical interfaces may further provide useful architectural blueprints. For example, to balance mass transport and surface protection, a 3D bi-

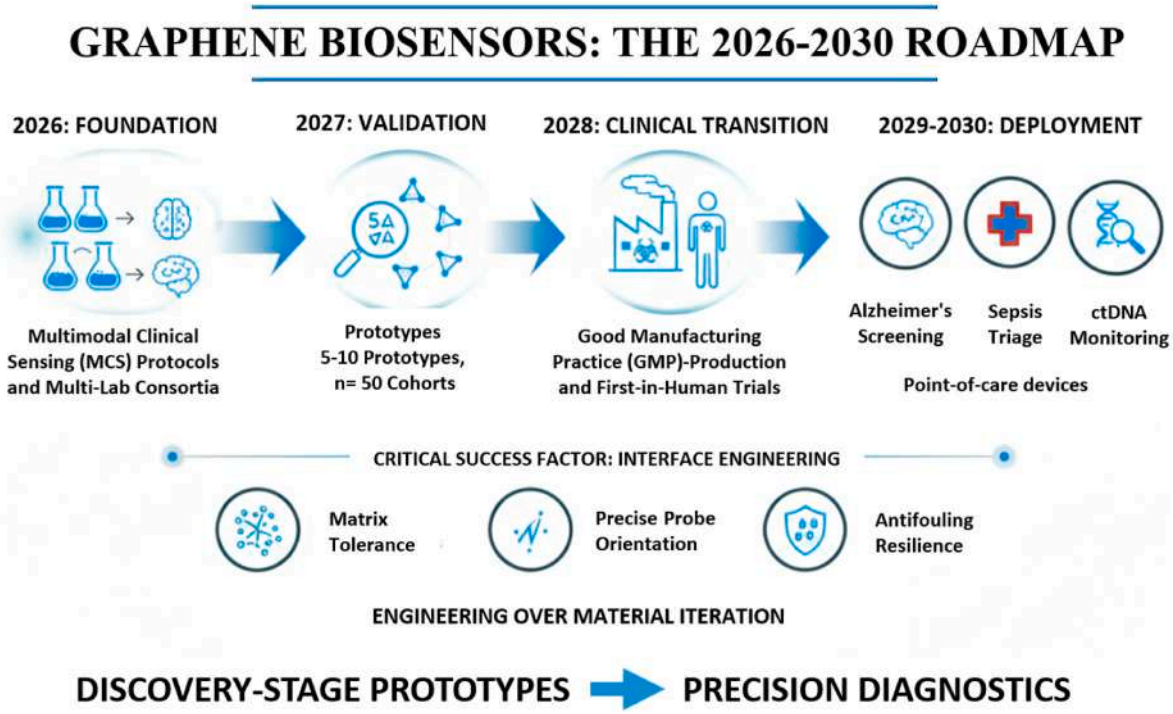

Fig. 10. Strategic roadmap for the clinical translation of graphene-based biosensors (2026-2030), according to graphene-innovation roadmaps and translational initiatives.

continuous nanoporous matrix, multi-arm PEG polymer brushes, and structure-switching aptamers were integrated to achieve week-long continuous in vivo tracking in whole blood. These multi-layered design principles may guide the design of 2D graphene interfaces that balance mass transport, target recognition, and fouling resistance (Chen et al., 2025).

However, the implementation of multi-layer interfaces presents a unique challenge for GFETs due to electrostatic screening constraints. Unlike electrochemical sensors, GFET sensitivity is governed by the Debye length, which is typically ~0.7–1 nm in physiological media (Gao et al., 2016). If the total thickness of this interface exceeds the effective Debye length, the electrostatic signal of the target analyte is effectively screened by mobile ions, leading to significant signal attenuation. Consequently, GFET-based designs require a delicate balance, providing sufficient matrix protection while maintaining an ultra-thin profile to ensure recognition occurs within the effective transduction zone.

Overall, the data support the conclusion that robustness in complex media is most likely to emerge from integrated interfaces that jointly manage transport, binding geometry, and fouling. Fully multi-analyte demonstrations of such coordinated architectures remain limited, which makes systematic co-design studies an important next step.

Accordingly, future research should focus on predictive co-optimization frameworks that evaluate the interplay among porosity, probe tilt angle, and interfacial hydration. The development of quantitative interface descriptors will be vital for sustaining multi-week stability while maintaining ultralow LODs in undiluted clinical samples. Overall, coordinated graphene interface engineering represents a compelling direction for enhancing the durability, reproducibility, and clinical relevance of next-generation biosensing.

5. Challenges and future outlook

Graphene-based biosensors have achieved substantial advances in sensitivity, probe orientation, and interfacial engineering. As the field moves toward clinical translation, the emphasis is shifting from demonstrating ultralow LODs in buffered systems to reliable and reproducible performance in complex biological and environmental matrices. This transition reflects the maturation of the field from material-level optimization to rigorous system-level validation.

In clinically relevant fluids such as plasma and serum, dynamic interfacial processes, including protein-corona formation, diffusion constraints, and electrostatic screening govern signal stability over time. Although porous matrices, vertically structured electrodes, and antifouling chemistries have improved signal retention under matrix exposure, long-term robustness under continuous flow, enzymatic activity, and in vivo conditions remains an active area of refinement (Son et al., 2026). Furthermore, high-performance nanostructured architectures must be adapted to scalable, International Organization for Standardization (ISO)-compliant, and regulatory-friendly manufacturing practices.

As architectural diversity expands, the need for standardized comparisons across studies becomes increasingly important. Matrix conditions such as albumin concentration, protease exposure, interferent composition, temperature, dilution state, and incubation duration all vary considerably throughout the literature, making direct performance comparisons difficult. The development of harmonized testing frameworks could therefore provide shared analytical benchmarks, enabling more objective evaluation of linker chemistries, antifouling strategies, and probe configurations while also facilitating future regulatory alignment.

Another priority is systematic multi-parameter optimization. Probe density influences steric accessibility, antifouling layers affect electrostatic screening, and nanostructure geometry governs how quickly analytes reach the active interface. Consequently, future studies should pursue and evaluate these variables together instead of focusing on single-parameter optimizations. In addition, the increasing complexity of interfacial architectures motivates the introduction of measurable design descriptors. Metrics such as orientation efficiency, signal-retention indices, and matrix-tolerance factors could enable more predictive comparison across platforms. Complementary computational approaches, including molecular-dynamics simulations of linker adsorption and data-guided exploration of steric-crowding limits, will be

essential for navigating the expanding design space while remaining grounded in experimental validation.

In this direction, various proposed translational initiatives, including programs under the EU Graphene Flagship and Horizon Europe, show growing coordination between laboratory innovation and clinical implementation. The 2026-2030 roadmap (Fig. 10), prepared from publicly available data of such initiatives, reflects a staged progression from harmonized sensing protocols to pilot validation and ISO 13485-compliant manufacturing, ultimately supporting point-of-care deployment across prioritized areas, such as neurological, infectious, and oncological applications ("EU Graphene Flagship"; "Horizon Europe's CombiDiag project"; "SIO Grafen").

A high-performance graphene biosensor should now be defined by sensitivity, along with robustness in complex matrices, batch-to-batch reproducibility, and compatibility with scalable fabrication. Continued progress is likely to emerge from interface-integrated engineering, standardized evaluation practices, and computationally informed design, thereby supporting the steady translation of graphene-based platforms into reliable sample-to-answer diagnostic technologies.

CRediT authorship contribution statement

Kalyan Vaid: Conceptualization, Visualization, Writing – original draft. **Indresh Verma:** Investigation, Writing – original draft. **Vishnu Pullagantil:** Investigation, Writing – original draft. **Radek Zboril:** Funding acquisition, Writing – review & editing. **Aristides Bakandritsos:** Conceptualization, Funding acquisition, Resources, Supervision, Visualization, Writing – review & editing.

Declaration of competing interest

The authors declare that they have no known competing financial interests or personal relationships that could have appeared to influence the work reported in this paper.

Acknowledgements

We acknowledge the funding from the European Union, under the HORIZON Europe, Grant Agreement 101120706 (project 2D-BioPAD). Views and opinions expressed are however those of the authors only and do not necessarily reflect those of the European Union or CNECT. We acknowledge the funding from the European Union under the REFRESH – Research Excellence for REgion Sustainability and High-tech Industries project number CZ.10.03.01/00/22_003/0000048 via the Operational Programme Just Transition, and the funding from the ERDF/ESF, project TECHSCALE No. CZ.02.01.01/00/22_008/0004587.

Data availability

No new data were generated for this review article.

References

Abrantes, M., Rodrigues, D., Domingues, T., Nemala, S.S., Monteiro, P., Borme, J., Alpuim, P., Jacinto, L., 2022. Ultrasensitive dopamine detection with graphene aptasensor multitransistor arrays. J. Nanobiotechnol. 20, 495. https://doi.org/10.1186/s12951-022-01695-0.

Amiri, S., Asghari, A., Vatanpour, V., Rajabi, M., 2020. Fabrication and characterization of a novel polyvinyl alcohol-graphene oxide-sodium alginate nanocomposite hydrogel blended PES nanofiltration membrane for improved water purification. Sep. Purif. Technol. 250, 117216. https://doi.org/10.1016/j.seppur.2020.117216.

Amiri, S., Vatanpour, V., He, T., 2023. Antifouling thin-film nanocomposite NF membrane with polyvinyl alcohol-sodium alginate-graphene oxide nanocomposite hydrogel coated layer for As(III) removal. Chemosphere 322, 138159. https://doi.org/10.1016/j.chemosphere.2023.138159.

Béraud, A., Sauvage, M., Bazán, C.M., Tie, M., Bencherif, A., Bouilly, D., 2021. Graphene field-effect transistors as bioanalytical sensors: design, operation and performance. Analyst 146, 403–428. https://doi.org/10.1039/D0AN01661F.

Breault-Turcot, J., Masson, J.-F., 2015. Microdialysis SPR: diffusion-gated sensing in blood. Chem. Sci. 6, 4247–4254. https://doi.org/10.1039/C5SC00716J.

Chen, Y., Fu, K.X., Cotton, R., Ou, Z., Kwak, J.W., Chien, J.-C., Kesler, V., Nyein, H.Y.Y., Eisenstein, M., Soh, H.T., 2025. A biochemical sensor with continuous extended stability in vivo. Nat. Biomed. Eng. 9, 1517–1530. https://doi.org/10.1038/s41551-025-01389-6.

Dauphin-Ducharme, P., Dief, E.M., Corcoran, N., Gooding, J.J., 2025. Reading the pulse of electrochemical aptamer-based biosensors: implications of different interrogation methods. ACS Electrochem 1, 2264–2275. https://doi.org/10.1021/acselectrochem.5c00316.

Demirkan, B., Bozkurt, S., Cellat, K., Arıkan, K., Yılmaz, M., Şavk, A., Çalımlı, M.H., Nas, M.S., Atalar, M.N., Alma, M.H., Sen, F., 2020. Palladium supported on polypyrrole/reduced graphene oxide nanoparticles for simultaneous biosensing application of ascorbic acid, dopamine, and uric acid. Sci. Rep. 10, 2946. https://doi.org/10.1038/s41598-020-59935-y.

Echeverri, D., Calucho, E., Marrugo-Ramírez, J., Álvarez-Diduk, R., Orozco, J., Merkoçi, A., 2024. Capacitive immunosensing at gold nanoparticle-decorated reduced graphene oxide electrodes fabricated by one-step laser nanostructuration. Biosens. Bioelectron. 252, 116142. https://doi.org/10.1016/j.bios.2024.116142.

EU Graphene Flagship, n.d. https://graphene-flagship.eu/(accessed 2 February 2026).

Fujita, H., Wan, L., Gidi, Y., Hein, L.A., Eisenstein, M., Soh, H.T., 2025. Discovery of high-specificity DNA aptamers for progesterone using a high-throughput array platform. bioRxiv. https://doi.org/10.1101/2025.09.13.675901.

Gao, N., Gao, T., Yang, X., Dai, X., Zhou, W., Zhang, A., Lieber, C.M., 2016. Specific detection of biomolecules in physiological solutions using graphene transistor biosensors. Proc. Natl. Acad. Sci. U. S. A 113, 14633–14638. https://doi.org/10.1073/pnas.1625010114.

Gong, J., Tang, H., Luo, X., Zhou, H., Lin, X., Wang, K., Yan, F., Xi, F., Liu, J., 2021. Vertically ordered mesoporous silica-nanochannel film-equipped three-dimensional macroporous graphene as sensitive Electrochemiluminescence platform. Front. Chem. 9, 770512. https://doi.org/10.3389/fchem.2021.770512. https://www.frontiersin.org/articles/10.3389/fchem.2021.770512/full. (Accessed 22 November 2021).

Horizon Europe's CombiDiag project, n.d. https://cordis.europa.eu/project/id/101071485/results (accessed 2 February 2026).

Ilyas, H., Shawuti, S., Siddiq, M., Niazi, J.H., Qureshi, A., 2019. PEG functionalized graphene oxide-silver nano-additive for enhanced hydrophilicity, permeability and fouling resistance properties of PVDF-co-HFP membranes. Colloids Surf. A Physicochem. Eng. Asp. 579, 123646. https://doi.org/10.1016/j.colsurfa.2019.123646.

Jakubec, P., Panáček, D., Nalepa, M., Rossetti, M., Álvarez-Diduk, R., Merkoçi, A., Vasjari, M., Kulla, L., Otyepka, M., 2025. Graphene derivatives as efficient transducing materials for covalent immobilization of biocomponents in electrochemical biosensors. Chem Electro Chem 12. https://doi.org/10.1002/celc.202400660 celc.202400660.

Jarosińska, E., Zambrowska, Z., Nery, E.W., 2024. Methods of protection of electrochemical sensors against biofouling in cell culture applications. ACS Omega 9, 4572–4580. https://doi.org/10.1021/acsomega.3c07660.

Jashrapuria, K., Singh, S.P., 2023. Zwitterionic polymer brush functionalized graphene oxide blended polyethersulfone membrane with enhanced performance and anti-biofouling properties. J. Membr. Sci. 687, 122032. https://doi.org/10.1016/j.memsci.2023.122032.

Khrapak, S., Khrapak, A., 2024. Stokes–einstein relation in different models of water. Molecules 29, 5587. https://doi.org/10.3390/molecules29235587.

Kumar, N., Gray, M., Ortiz-Marquez, J.C., Weber, A., Desmond, C.R., Argun, A., van Opijnen, T., Burch, K.S., 2020. Detection of a multi-disease biomarker in saliva with graphene field effect transistors. Med. Devices Sens. 3, e10121. https://doi.org/10.1002/mds3.10121.

Lee, J.-C., Kim, S.Y., Song, J., Jang, H., Kim, M., Kim, H., Choi, S.Q., Kim, S., Jolly, P., Kang, T., Park, S., Ingber, D.E., 2024. Micrometer-thick and porous nanocomposite coating for electrochemical sensors with exceptional antifouling and electroconducting properties. Nat. Commun. 15, 711. https://doi.org/10.1038/s41467-024-44822-1.

Lee, J.-H., Park, S.-J., Choi, J.-W., 2019. Electrical property of graphene and its application to electrochemical biosensing. Nanomaterials 9, 297. https://doi.org/10.3390/nano9020297.

Li, M., Zeng, Y., Huang, Z., Zhang, L., Liu, Y., 2023. Vertical graphene-based printed electrochemical biosensor for simultaneous detection of four Alzheimer's disease blood biomarkers. Biosensors 13, 758. https://doi.org/10.3390/bios13080758.

Li, X., Zou, D., Tong, L., Li, M., Dong, Y., Xu, S., Wang, Q., Wang, K., 2025. Bio-inspired MXene/graphene oxide-based nanocomposites with enhanced interfacial self-healing effects and multifunctional integration. Chem. Eng. J. 513, 162857. https://doi.org/10.1016/j.cej.2025.162857.

Liu, G., Lv, Z., Batool, S., Li, M., Zhao, P., Guo, L., Wang, Y., Zhou, Y., Han, S., 2023. Biocompatible material-based flexible biosensors: from materials design to wearable/implantable devices and integrated sensing systems. Small 19, 2207879. https://doi.org/10.1002/smll.202207879.

Liu, Y., Zhang, D., Ren, B., Gong, X., Xu, L., Feng, Z.-Q., Chang, Y., He, Y., Zheng, J., 2020. Molecular simulations and understanding of antifouling zwitterionic polymer brushes. J. Mater. Chem. B 8, 3814–3828. https://doi.org/10.1039/D0TB00520G.

Loo, A.H., Bonanni, A., Pumera, M., 2013. Biorecognition on graphene: physical, covalent, and affinity immobilization methods exhibiting dramatic differences. Chem. Asian J. 8, 198–203. https://doi.org/10.1002/asia.201200756.

Lv, N., Qiu, X., Han, Q., Xi, F., Wang, Y., Chen, J., 2022. Anti-biofouling electrochemical sensor based on the binary nanocomposite of silica nanochannel array and graphene for doxorubicin detection in human serum and urine samples. Molecules 27 (24), 8640. https://doi.org/10.3390/molecules27248640. https://www.mdpi.com/1420-3049/27/24/8640. (Accessed 7 December 2022).

Majeed, A.A., Gataa, I.S., Ibadi Alaridhee, Z.A., Alqaraguly, M.B., Ibrahim, S.K., Formanova, S., Abbas Al-Anbari, H.H., Jabir, M.S., Majdi, H., Zaki Fareed, Y.Y., Kariem, M., Abomughaid, M.M., 2025. A low-fouling electrochemical immunosensor based on reduced graphene oxide and terbium@amine-functionalized fibrous silica-modified screen-printed carbon electrodes for ratiometric detection of carcinoembryonic antigen (CEA) in serum samples. Microchem. J. 210, 112928. https://doi.org/10.1016/j.microc.2025.112928.

Meng, S., Liu, Y., Wang, L., Ji, X., Chen, Y., Zheng, T., Yu, J., Feng, H., 2021. Graphene-based flexible sensors for simultaneous detection of ascorbic acid, dopamine, and uric acid. Front. Bioeng. Biotechnol. 9, 726071. https://doi.org/10.3389/fbioe.2021.726071.

Novoselov, K.S., Falʹko, V.I., Colombo, L., Gellert, P.R., Schwab, M.G., Kim, K., 2012. A roadmap for graphene. Nature 490, 192–200. https://doi.org/10.1038/nature11458.

Oishi, Y., Ogi, H., Hagiwara, S., Otani, M., Kusakabe, K., 2022. Theoretical analysis on the stability of 1-pyrenebutanoic acid succinimidyl ester adsorbed on graphene. ACS Omega 7, 31120–31125. https://doi.org/10.1021/acsomega.2c03257.

Parolo, C., Sena-Torralba, A., Bergua, J.F., Calucho, E., Fuentes-Chust, C., Hu, L., Rivas, L., Álvarez-Diduk, R., Nguyen, E.P., Cinti, S., Quesada-González, D., Merkoçi, A., 2020. Tutorial: design and fabrication of nanoparticle-based lateral-flow immunoassays. Nat. Protoc. 15, 3788–3816. https://doi.org/10.1038/s41596-020-0357-x.

Pellitero, M.A., Curtis, S.D., Arroyo-Currás, N., 2021. Interrogation of electrochemical aptamer-based sensors via peak-to-peak separation in cyclic voltammetry improves the temporal stability and batch-to-batch variability in biological fluids. ACS Sens. 6, 1199–1207. https://doi.org/10.1021/acssensors.0c02455.

Ramadan, S., Lobo, R., Zhang, Y., Xu, L., Shaforost, O., Kwong Hong Tsang, D., Feng, J., Yin, T., Qiao, M., Rajeshirke, A., Jiao, L.R., Petrov, P.K., Dunlop, I.E., Titirici, M.-M., Klein, N., 2021. Carbon-dot-enhanced graphene field-effect transistors for ultrasensitive detection of exosomes. ACS Appl. Mater. Interfaces 13, 7854–7864. https://doi.org/10.1021/acsami.0c18293.

Russo, M.J., Han, M., Desroches, P.E., Manasa, C.S., Dennaoui, J., Quigley, A.F., Kapsa, R.M.I., Moulton, S.E., Guijt, R.M., Greene, G.W., Silva, S.M., 2021. Antifouling strategies for electrochemical biosensing: mechanisms and performance toward point of care based diagnostic applications. ACS Sens. 6, 1482–1507. https://doi.org/10.1021/acssensors.1c00390.

Sabaté del Río, J., Henry, O.Y.F., Jolly, P., Ingber, D.E., 2019. An antifouling coating that enables affinity-based electrochemical biosensing in complex biological fluids. Nat. Nanotechnol. 14 (12), 1143–1149. https://doi.org/10.1038/s41565-019-0566-z. https://www.nature.com/articles/s41565-019-0566-z. (Accessed 11 November 2019).

Sackmann, E.K., Fulton, A.L., Beebe, D.J., 2014. The present and future role of microfluidics in biomedical research. Nature 507, 181–189. https://doi.org/10.1038/nature13118.

Saxena, S., Sen, P., Soleymani, L., Hoare, T., 2024. Anti-fouling polymer or peptide-modified electrochemical biosensors for improved biosensing in complex media. Adv. Sens. Res. 3, 2300170. https://doi.org/10.1002/adsr.202300170.

Schuck, A., Kim, H.E., Moreira, J.K., Lora, P.S., Kim, Y.-S., 2021. A graphene-based enzymatic biosensor using a common-gate field-effect transistor for L-lactic acid detection in blood plasma samples. Sensors 21, 1852. https://doi.org/10.3390/s21051852.

Shahriari, S., Panjikar, S., Raman, R.S., Sastry, M., 2026. Immobilisation of bovine serum albumin on graphene oxide through covalent and noncovalent interactions. Colloids Surf. B Biointerfaces 258, 115203. https://doi.org/10.1016/j.colsurfb.2025.115203.

Sharma, A., Wulff, A., Thomas, A., Sonkusale, S., 2024. Ultrasensitive electrochemical sensor for detection of salivary cortisol in stress conditions. Microchim. Acta 191, 103. https://doi.org/10.1007/s00604-023-06169-0.

SIO Grafen, n.d. https://www.vinnova.se/en/p/sio-grafen-roadmap-manufacturing/(accessed 2 February 2026).

Soman, G., M, V., Hedge, G., 2023. Molecularly imprinted graphene based biosensor as effective tool for electrochemical sensing of uric acid. Sens. Int. 4, 100243. https://doi.org/10.1016/j.sintl.2023.100243.

Son, K., Gibson, J.M., Gerson, J., Leung, K.K., Stocco, M., Lu, Y., Kippin, T.E., Plaxco, K. W., 2026. Continuous, week-long, seconds-resolved in vivo drug measurements performed with a xenonucleic acid-employing electrochemical, aptamer-based sensor. J. Am. Chem. Soc. 148, 10016–10025. https://doi.org/10.1021/jacs.5c22605.

Turner, A.P.F., 2013. Biosensors: sense and sensibility. Chem. Soc. Rev. 42, 3184. https://doi.org/10.1039/c3cs35528d.

Wang, B., Wang, P., He, B., Ma, S., Liu, S., Ye, Q., Zhou, F., 2023. Zwitterionic polymer brush-functionalized dual-crosslinked hydrogel via subsurface-initiated atom transfer radical polymerization for anti-fouling applications. Prog. Org. Coat. 183, 107729. https://doi.org/10.1016/j.porgcoat.2023.107729.

Wang, C., Cui, X., Li, Y., Li, H., Huang, L., Bi, J., Luo, J., Ma, L.Q., Zhou, W., Cao, Y., Wang, B., Miao, F., 2016. A label-free and portable graphene FET aptasensor for children blood lead detection. Sci. Rep. 6, 21711. https://doi.org/10.1038/srep21711.

Wang, X., Zhu, Y., Olsen, T.R., Sun, N., Zhang, W., Pei, R., Lin, Q., 2018. A graphene aptasensor for biomarker detection in human serum. Electrochim. Acta 290, 356–363. https://doi.org/10.1016/j.electacta.2018.08.062.

Wang, Y.-T., Mukundan, A., Karmakar, R., Chen, T.-H., Dhiman, H., Lin, F.-M., Wang, H.-C., 2025. A comprehensive review of graphene-based biosensors: fabrication, applications, characterization and future perspectives—A review. APL Bioeng. 9, 031504. https://doi.org/10.1063/5.0266596.

Wang, Z., Dai, W., Zhang, Z., Wang, H., 2025. Aptamer-based graphene field-effect transistor biosensor for cytokine detection in undiluted physiological media for cervical carcinoma diagnosis. Biosensors 15, 138. https://doi.org/10.3390/bios15030138.

Xu, L., Ramadan, S., Rosa, B.G., Zhang, Y., Yin, T., Torres, E., Shaforost, O., Panagiotopoulos, A., Li, B., Kerherve, G., Kim, D.K., Mattevi, C., Jiao, L.R., Petrov, P. K., Klein, N., 2022. On-chip integrated graphene aptasensor with portable readout for fast and label-free COVID-19 detection in virus transport medium. Sens. Diagn 1, 719–730. https://doi.org/10.1039/D2SD00076H.

Yin, T., Xu, X., Huang, Z., Rosa, B.G., Gaboriau, D.C.A., Merali, N., Keshavarz, M., Bin Muhammad Mustafa, A.N., Song, J., Alodan, S., Petrov, P.K., Frampton, A.E., Skinner, S.J., Alford, N., Hu, Y., Ramadan, S., Klein, N., 2025. Control of antibody orientation on graphene using porphyrin linker molecules for high-performance graphene-based immuno-biosensors. J. Am. Chem. Soc. 147, 47638–47653. https://doi.org/10.1021/jacs.5c17186.

Zambrano, A.C., Loiola, L.M.D., Bukhamsin, A., Gorecki, R., Harrison, G., Mani, V., Fatayer, S., Nunes, S.P., Salama, K.N., 2024. Porous laser-scribed graphene electrodes modified with zwitterionic moieties: a strategy for antibiofouling and low-impedance interfaces. ACS Appl. Mater. Interfaces 16, 4408–4419. https://doi.org/10.1021/acsami.3c15849.

Zhang, L., Li, C., Yang, Y., Han, J., Huang, W., Zhou, J., Zhang, Y., 2022. Anti-biofouling Ti3C2TX MXene-holey graphene modified electrode for dopamine sensing in complex biological fluids. Talanta 247, 123614. https://doi.org/10.1016/j.talanta.2022.123614.

Zhang, W., Huang, H., Bernstein, R., 2022. Zwitterionic hydrogel modified reduced graphene oxide/ZnO nanocomposite blended membrane with high antifouling and antibiofouling performances. J. Colloid Interface Sci. 613, 426–434. https://doi.org/10.1016/j.jcis.2021.12.194.

Zhang, W., Jia, B., Furumai, H., 2018. Fabrication of graphene film composite electrochemical biosensor as a pre-screening algal toxin detection tool in the event of water contamination. Sci. Rep. 8, 10686. https://doi.org/10.1038/s41598-018-28959-w.

Zhao, S., Yang, J., Wang, L., Dong, B., Mao, Y., Qu, H., Zheng, L., 2023. Selective detection of Pb2+ ions based on a graphene field-effect transistor gated by DNAzymes in binding mode. Biosens. Bioelectron. 237, 115549. https://doi.org/10.1016/j.bios.2023.115549.

Zhu, C., Wang, H., Liu, J., 2025. Highly sensitive electrochemical immunosensor based on methylene blue-reduced graphene oxide nanocomposites as signal probes for IL-6 detection in gingival crevicular fluid samples. Front. Chem. 13, 1549927. https://doi.org/10.3389/fchem.2025.1549927.

Zinggeler, M., Schär, S., Kurth, F., 2022. Printed antifouling electrodes for biosensing applications. ACS Appl. Mater. Interfaces 14, 56578–56584. https://doi.org/10.1021/acsami.2c17557.

Zupančič, U., Jolly, P., Estrela, P., Moschou, D., Ingber, D.E., 2021. Graphene enabled low-noise surface chemistry for multiplexed sepsis biomarker detection in whole blood. Adv. Funct. Mater. 31 (16), 2010638. https://doi.org/10.1002/adfm.202010638. https://advanced.onlinelibrary.wiley.com/doi/10.1002/adfm.202010638. (Accessed 12 February 2021).